Available online at www.sciencedirect.com

ScienceDirect

Procedia Engineering 126 (2015) 24 – 28

Procedia Engineering

www.elsevier.com/locate/procedia

7th International Conference on Fluid Mechanics, ICFM7

An extended view of the inner-outer interaction model for wall-bounded turbulence using spectral linear stochastic estimation

Ivan Marusic*, Woutijn J. Baars, Nicholas Hutchins

Department of Mechanical Engineering, The University of Melbourne, Parkville, Victoria 3010, Australia

Abstract

Streamwise velocity fluctuations in the inner-region of wall-bounded turbulent flows can be predicted by the model of Marusic, Mathis & Hutchins (2010). Only a single large-scale velocity signal from an outer position in the logarithmic region is needed for the model, and all other parameters are determined from a once-off calibration experiment. Here we elucidate part of the model by investigating the scale-dependent coherence magnitude and phase throughout the boundary layer. The collection of coherent scales exhibits a shift with respect to the reference position that is shown to be independent of scale; thus the large-scales are non-dispersive. Because these scales comprise a strong coherence, their signature in the inner-region is predicted from an input signal acquired at the geometric center of the log-region. Previously this was achieved via *single-time* stochastic estimation. Here we leverage the inherent advantages of *spectral* linear stochastic estimation for the prediction of these large-scales.

Peer-review under responsibility of The Chinese Society of Theoretical and Applied Mechanics (CSTAM)

Keywords: wall-turbulence; coherent structures; scale-interaction; linear stochastic estimation

1. Introduction

Several decades of research on high-Reynolds-number wall-bounded turbulent flows has revealed an organization of large-scale turbulent structures that is most pronounced in the logarithmic region. The large-scale coherence is evidenced by structures that comprise significant lifetimes in the streamwise direction, an organization in the spanwise direction, and a hierarchical ordering of scales in the wall-normal direction [1,2,3; among others]. This coherence is illustrated when considering the scale-dependent coherence between the streamwise velocity fluctuations u of two synchronously acquired single-hot-wire anemometry probes in a turbulent boundary layer

* Corresponding author. Tel.: +61 3 8344 7717; fax: + 61 3 8344 4290
E-mail address: imarusic@unimelb.edu.au

Peer-review under responsibility of The Chinese Society of Theoretical and Applied Mechanics (CSTAM)
doi:10.1016/j.proeng.2015.11.171

(TBL). Here we consider data taken in a TBL with a friction Reynolds number of $Re_\tau = u_\tau \delta/\nu = 14{,}750$ ($u_\tau = 0.626 ms^{-1}$ and $\delta = 0.361m$). A fixed near-wall probe was employed at a wall-normal position of $z^+ = z\,u_\tau/\nu \approx 4.3$ and a traversing hot-wire spanned forty positions ranging from $z^+ = 10.5$ to $z/\delta = 1.45$; the experiments were performed at the high-Reynolds number boundary layer facility at the University of Melbourne with equipment described elsewhere [*e.g.* 3, 4]. The coherence *magnitude* is presented in terms of the linear coherence spectrum, denoted as γ [5], and is computed from the complex-valued cross-spectrum $S_{IO} = \langle U_I^+(z^+;\lambda_x^+)\overline{U_O^+(z_O^+;\lambda_x^+)}\rangle$ and the power spectra S_{II} and S_{OO} according to the LHS expression in Eq. (1). Here, 'I' and 'O' refer to the inner- and outer-probe, respectively, and $U^+(z^+;\lambda_x^+) = \mathcal{F}[u^+(z^+,t^+)]$ is the Fourier transform of u.

$$\gamma_{IO}\left(\lambda_x^+\right) = \left|S_{IO}\left(\lambda_x^+\right)\right|^2 \Big/ \left(S_{II}\left(\lambda_x^+\right)S_{OO}\left(\lambda_x^+\right)\right), \quad \varphi_{IO}\left(\lambda_x^+\right) = \tan^{-1}\left(\Im\left[S_{IO}\left(\lambda_x^+\right)\right]\Big/\Re\left[S_{IO}\left(\lambda_x^+\right)\right]\right) \tag{1}$$

The RHS expression in Eq. (1) is the radial phase φ of the scale-dependent cross-spectrum. Note that the local mean velocity is used when transforming frequency to inner-scaled wavelength λ_x^+. Coherence spectra for u between the near-wall probe and the traversing probe are shown in Fig. 1a. Underlying the coherence magnitude is the spectrogram of the traversing wire; the position of the near-wall wire (coherence reference position) is shown with the dash-dot line. The observed trend is consistent with the framework of Townsend's attached eddy-hypothesis; *e.g.* only larger scales remain coherent with the inner-region when moving away from the wall through the log-region. The phase for the coherent scales is shown in Fig. 1b. The temporal shift is expressed in outer-scaled time shift $\tau\,U_\infty/\delta$, where a negative τ implies a lag of the wall-wire w.r.t. the traversing probe. It is evident that the temporal shift is only weakly dependent on scale; the large-scales are non-dispersive. Similar observations were made when the fixed probe was positioned in the geometric center of the log-region.

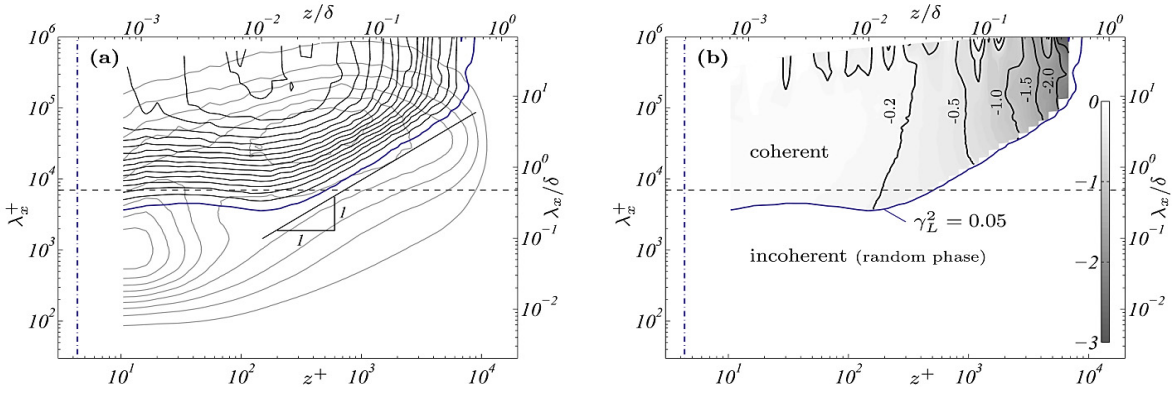

Fig. 1. (a) Coherence magnitude for the streamwise velocity fluctuations u relative to the near-wall probe (black contour, level range 0.05—0.95, level step 0.05). Underlying is the spectrogram of the pre-multiplied energy spectra $k_x\,\phi_{uu}/u_\tau^2$ (grey contour, level range 0.2—1.8, level step 0.2). (b) Scale-dependent shift between the wire positions (phase of coherence) expressed in outer-scaled time shift $\tau\,U_\infty/\delta$.

Previously, Mathis *et al.* [4] recognized that small-scale fluctuations are modulated by the large-scale coherent events. This led to the development of a predictive model for turbulence statistics in the inner-region and was derived for the fluctuating streamwise velocity [4, 6-7] and is known as the Inner-Outer Interaction Model (IOIM). The near-wall fluctuating velocity signal $u_p^+(z^+,t^+)$ at inner position $z^+$is predicted given a large-scale input signal u_{OL}^+ at position z_O^+ in the outer layer, according to the two-segment expression given by Eq. (2).

$$u_p^+\left(z^+,t^+\right) = u^*\left(z^+,t^+\right)\left\{1+\beta u_{OL}^+\left(z_O^+,\theta_L,t^+\right)\right\} + \alpha u_{OL}^+\left(z_O^+,\theta_L,t^+\right) \tag{2}$$

The first part encompasses an amplitude modulation of a universal signal u^*, where the large-scale input acts as the modulation envelope. The second part models the direct influence of the large-scale events at the wall through superposition. Signal u^* and coefficients α, β, and θ_L are obtained through a calibration experiment [7]. When we

focus on the superposition part of the model two coefficients are of relevance, being α and θ_L, and are both functions of prediction location z^+ for a fixed outer-layer position z_O^+ of the model's input. The calibration procedure for obtaining $\alpha(z^+)$ and $\theta(z^+)$ involves the synchronous acquisition of $u^+(z^+)$ in the inner-region and $u_O^+(z_O^+)$ in the log-region. A long-wavelength pass-filter is then employed to extract their large-scale signatures: $u_L^+(z^+)$ and $u_{OL}^+(z_O^+)$. This scale decomposition requires a cut-off wavelength to be selected (typically taken as $\lambda_x^+ = 7{,}000$) and is assumed to be invariant with Reynolds number [3-4]. Parameters α and θ_L are obtained from the correlation of the two large-scale signals and α is taken as the maximum of the normalized temporal cross-correlation coefficient α' scaled by the ratio of standard deviations: $\alpha = \alpha'\,\sigma(u_L^+)/\sigma(u_{OL}^+)$. The time shift τ at which that maximum occurs is expressed as a physical inclination angle $\theta_L = \tan^{-1}[d/(\tau u_c)]$, where d is the wire-separation distance and u_c is the mean velocity at z_O^+. And so, the aforementioned superposition $\alpha u_{OL}^+(\theta_L)$ implies that the large-scale component is imposed on the near-wall prediction through a procedure of scaling its amplitude and shifting the entire signal u_{OL}^+ with one temporal shift. In the context of stochastic estimation it is apparent that this condenses to single-time Linear Stochastic Estimation (LSE). In the past several decades, stochastic estimation techniques have been applied extensively to coherent turbulent flows to study their structure [8]. In particular, it has been shown that multi-time LSE (effectively a frequency-domain approach) results in a better estimate than the single-time LSE [9-10]; see also the overview in [11]. Spectral LSE as described by Tinney *et al*. [12] performs the multi-time estimate efficiently in the frequency-domain and is associated with reduced complexity. Furthermore, sLSE eliminates the selection of a cut-off wavelength to decompose the signal in small- and large-scales, since this is implicitly accounted for during the sLSE procedure. Henceforth, we aim to replace the superposition part of the model by sLSE. The spectral approach is also convenient for implementing the IOIM in large-eddy simulation (LES). Recently, a similar model for predicting wall-shear stress fluctuations [13] was implemented in LES [14].

2. Refined superposition component for IOIM

A short overview of the model refinement using sLSE is now provided. From the perspective of signal processing, the signals $u_O^+(z_O^+)$ and $u^+(z^+)$ form the input and output of a black-box physical system, respectively. For a single input at the geometric center of the log-region ($z_O^+ = 3.9Re_\tau^{0.5} \approx 469$) and output location near the wall ($z^+ = 10.5$) in a $Re_\tau = 14{,}900$ TBL, the scale-dependent coherence is shown in Fig. 2a, according to Eq. (1). As seen previously, the large-scales are coherent with an amplitude of ≈ 0.8 for large wavelengths. Now the sLSE procedure requires the ensemble-averaged linear transfer function to be computed according to Eq. (3).

$$H_L(\lambda_x^+) = \frac{S_{IO}(\lambda_x^+)}{S_{OO}(\lambda_x^+)} = \left|H_L(\lambda_x^+)\right| \exp\left[\phi(\lambda_x^+)\right] \tag{3}$$

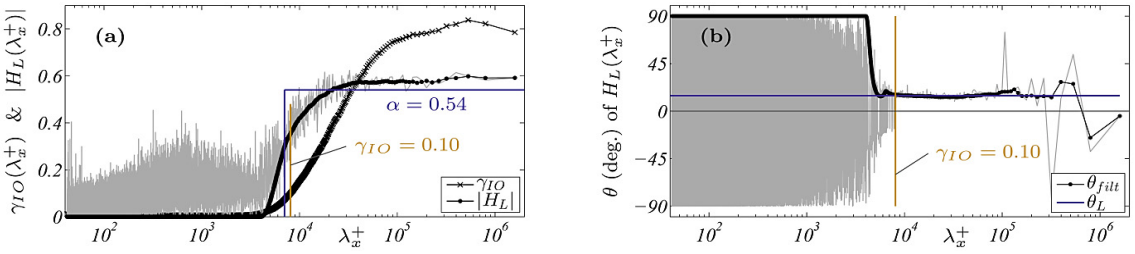

Fig. 2. (a) Coherence magnitude γ and linear transfer gain $|H_L|$ of the streamwise velocity fluctuations between a single inner- ($z^+ = 10.5$) and outer-region ($z_O^+ = 469$) signal. (b) Scale-dependent linear transfer phase, expressed in terms of a physical inclination angle.

Gain $|H_L|$ of this complex-valued transfer function is also shown in Fig. 2a, where the grey line reflects the unfiltered gain and the black line indicates the filtered gain with a bandwidth moving filter of 10%. Since there is an absence of coherence at small wavelengths, the filtered transfer function is subsequently set to zero using a smooth roll-off whenever the normalized coherence is below a threshold of 0.1; the results are insensitive to such a

threshold due to the clear natural decay trend in the coherence. For the readers perusal we have also indicated the scaling coefficient of the superposition part in the IOIM, $\alpha = 0.54$, and the cut-off wavelength at $\lambda_x^+ = 7{,}000$ (blue rectangle). The transfer gain is an analogy of a scale-dependent coefficient α, and in comparing $|H_L|$ and α it is notable that a constant α for the range $\lambda_x^+ > 7{,}000$ is a reasonable simplification of the true –empirically derived– transfer function. Concerning the phase of the large-scales, we have plotted the scale-dependent phase ϕ of the transfer function in Fig. 2b after transforming the radial phase to a physical inclination angle, so that we could compare it to the scale-independent physical inclination angle of the conventional IOIM ($\theta_L = 14.6°$). Again, a constant temporal shift is a reasonable assumption for these non-dispersive scales

Moving forward with the refinement of the IOIM we can replace coefficients α and θ_L with the frequency-dependent linear transfer kernel, $H_L(\lambda_x^+) \in \mathbb{C}$, which is a function of the wavelength and location z^+. In doing this, all coherent large-scales are weighted properly in the estimate, and, their scale-dependent phase is efficiently accounted for in one single computation in frequency space. Henceforth, the second part in Eq. (1) becomes the inverse Fourier transform of the frequency-domain estimate, given by Eq. (4).

$$\hat{u}^+\left(z^+,t^+\right) = F^{-1}\left\{\hat{U}^+\left(z^+;\lambda_x^+\right)\right\} = F^{-1}\left\{H_L\left(z^+;\lambda_x^+\right)F\left[u_O^+\left(z_O^+,t^+\right)\right]\right\} \tag{4}$$

The estimates of the large-scale signature at the wall, for the same inner- and outer-region signals used to construct Fig. 2, are shown in Fig. 3. Both estimates following from the refined sLSE and conventional single-time LSE are shown alongside the unfiltered measured signal at z^+ (Fig. 3a). For reference, the sLSE estimate and the long-wavelength pass-filtered signal of the true measurement are compared in Fig. 3b. The high-pass filter was constructed from the linear gain $|H_L(\lambda_x^+)|$ such that we could again avoid the choice of a cut-off wavelength. The small difference in the predictions shown in Fig. 3a and Fig. 2 are an illustration of why single-time LSE in the original model results in satisfactory predictions (discrepancies would have been larger for more dispersive fields).

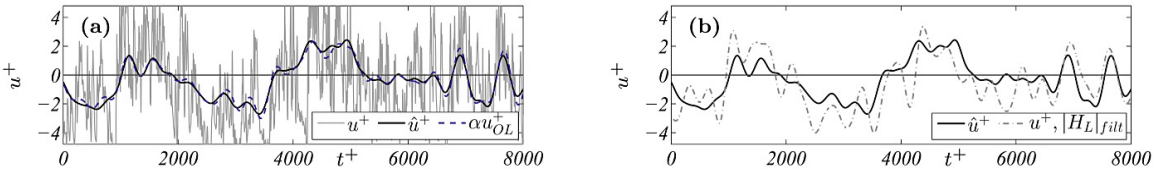

Fig. 3. (a) Streamwise velocity fluctuations at $z^+ = 10.5$; measured (u^+), sLSE ($\hat{u}^+$) and single-time LSE (αu_{OL}^+). (b) Comparison of $\hat{u}^+$ and the true measurement u^+ filtered according to the linear transfer gain.

3. New set of model calibration parameters

Following the sLSE procedure outlined in §2 we can update the IOIM equation, Eq. (2), so that it reflects the new superposition component obtained in Eq. (4); the new IOIM equation is given by Eq. (5).

$$u_p^+\left(z^+,t^+\right) = u^*\left(z^+,t^+\right)\left\{1+\Gamma\hat{u}^+\left(z^+,t^+\right)\right\} + \hat{u}^+\left(z^+,t^+\right) \tag{5}$$

Since the model's input signal of the outer-layer is also present in the modulation part, we have replaced this by the superposition estimate. To avoid an ambiguous use of coefficients, we have replaced the original demodulation coefficient β in the modulation part by Γ, so that this coefficient equates to parameter group β/α of the former model expression. It is important to emphasize that the only input to Eqs. (4,5) is the unfiltered (raw) signal acquired in the log-region: $u_O^+(z_O^+,t^+)$. Two advantages of utilizing sLSE for superimposing the large-scale signature on the near-wall prediction can therefore be summarized as follows. First, the time shift between the inner- and outer-region signals, previously formulated as θ_L, is not uniquely defined. The spectral technique avoids this scale-dependent phase ambiguity, since the phase state of the signals are naturally preserved by the spectral estimation coefficients $H_L(z^+;\lambda_x^+) \in \mathbb{C}$, and eliminates the burden of having to identify a single streamwise shift. Secondly, applying sLSE eliminates the need for a scale decomposition that requires the choice of a cut-off wavelength

typically taken as $\lambda_x^+ = 7{,}000$. The large-scale coherent signature is implicitly extracted from the input through the scale-dependent gain $|H_L(\lambda_x^+)|$, which can be interpreted as an empirically derived scale-filter. On a final note regarding the extraction of the universal signal during the model calibration [7], it is required to compute the amplitude modulation coefficient [4] which requires a long-wavelength pass-filter. This filter is constructed from gain $|H_L(\lambda_x^+)|$ such that we again avoid the choice of a cut-off wavelength. While the previous form of the model, Eq. (2), required calibration parameters α, β, θ_L and universal signal u^*, the new form, Eqs. (4,5) requires H_L, Γ, and u^*. The new parameters extracted from a calibration experiment at $Re_\tau = 14{,}900$ are shown in Figs. 4a,b & c, respectively. Here, only the transfer *gain* is shown and the *spectrogram* of the universal signal. The transfer kernel is a function of the inner-scaled prediction location and inner-scaled wavelength λ_x^+. It is important to realize that the spectral properties of the universal signal are marginally changed, relative to the former model, due to our utilization of all available large-scale coherence during the sLSE procedure for obtaining the superposition signature.

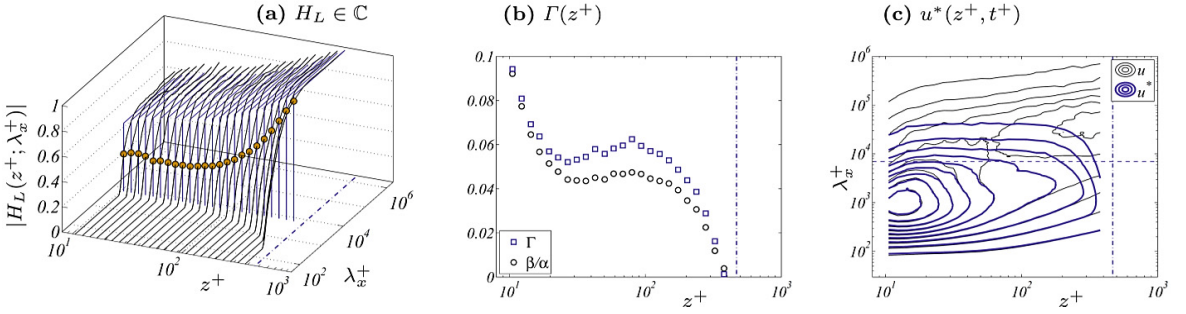

Fig. 4. (a) Wall-normal evolution of the wavelength-dependent linear transfer gain (black lines); blue lines indicate coefficient α up to $\lambda_x^+ = 7{,}000$. (b) Wall-normal evolution of coefficient Γcompared to the parameter group β/α of the former calibration method. (c) Pre-multiplied energy spectra of the streamwise velocity fluctuation $k_x \phi_{uu}/u_\tau^2$ for the acquired calibration signal u and universal signal u^*.

Acknowledgements

The authors wish to gratefully acknowledge the Australian Research Council for financial support. The authors would like to give special thanks to Dougal T. Squire for his assistance during the experimental campaign.

References

[1] R.F. Blackwelder, L.S.G. Kovasznay, Time scales and correlations in a turbulent boundary layer, Phys. Fluids 15:9 (1972), pp. 1545–1554.
[2] K.C. Kim, R.J. Adrian, Very large-scale motion in the outer layer, Phys. Fluids 11:2 (1999), pp. 417–422.
[3] N. Hutchins, I. Marusic, Large-scale influences in near-wall turbulence, Phil. Trans. R. Soc. A 365 (2007), pp. 747–664.
[4] R. Mathis, N. Hutchins, I. Marusic, Large-scale amplitude modulation of the small-scale structures in turbulent boundary layers, J. Fluid Mech. 628 (2009), pp. 311–337.
[5] J.S. Bendat, A.G. Piersol, Random data: analysis and measurement procedures, John Wiley & Sons, Inc. (2000). pp. 2941–2949.
[6] I. Marusic, R. Mathis, N. Hutchins, Predictive model for wall-bounded turbulent flow, Science 329:5988 (2010), pp. 193–196.
[7] R. Mathis, N. Hutchins, I. Marusic, A predictive inner–outer model for streamwise turbulence statistics in wall-bounded flows, J. Fluid Mech. 681 (2011) pp. 537–566.
[8] R.J. Adrian, Conditional eddies in isotropic turbulence, Phys. Fluids 22:11 (1979), pp. 2065–2070.
[9] D. Ewing, J. Citriniti, Examination of LSE/POD complementary technique using single and multi-time information in the axisymmetric shear layer, In *Proc. IUTAM Symp*., pp. 375–384. Lynby, Denmark, eds. J.N. Sorensen, E.J. Hopfinger, N. Aubry.
[10] D.R. Cole, M.N. Glauser, Applications of stochastic estimation in the axisymmetric sudden expansion, Phys. Fluids 10:11 (1998),
[11] W.J. Baars, C.E. Tinney, Proper orthogonal decomposition-based spectral higher-order stochastic estimation, Phys. Fluids 26 (2014), 055112.
[12] C.E. Tinney, F. Coiffet, J. Delville, M.N. Glauser, P. Jordan, A.M. Hall, On spectral linear stochastic estimation, Exp. Fluids 41:5 (2006) pp. 763–775.
[13] R. Mathis, I. Marusic, S.I. Chernyshenko, N. Hutchins, Estimating wall-shear-stress fluctuations given an outer region input, J. Fluid Mech. 715 (2013) pp. 163–180.
[14] W. Sidebottom, O. Cabrit, I. Marusic, C. Meneveau, A. Ooi, D. Jones, Modelling of wall shear-stress fluctuations for large-eddy simulation, In Proc. 19th Australasian Fluid Mechanics Conf., Melbourne, Australia (2014).